Arabian Journal for Science and Engineering (2019) 44:5647–5655
https://doi.org/10.1007/s13369-018-3678-0

RESEARCH ARTICLE - MECHANICAL ENGINEERING

Pressure-Driven Flow of Cross Fluid Along a Stationary Plate Subject to Binary Chemical Reaction and Arrhenius Activation Energy

M. Mustafa[1,2] · Aiman Sultan[1] · Mahmood Rahi[2]

Received: 25 June 2018 / Accepted: 4 December 2018 / Published online: 15 December 2018

Abstract

The present paper deals with the flow of Cross rheological fluid along a stationary rigid plate caused by stream-wise pressure gradient. Flow field is affected by uniform magnetic field acting normal to the plate axis. Interaction of flow field with chemically reacting solute is modeled through the advection–diffusion equation in which temperature dependency of the reaction rate on activation energy is considered. Energy equation containing source term and variable thermal conductivity is treated. Locally similar solutions are obtained and interpreted for a certain range of embedded parameters. Shear-thinning aspect of Cross fluid is apparent from the computational results. A monotonic decay in vertical velocity is noticed for increasing values of flow behavior index (n) which, in turn, leads to pronounced heat conduction. An important finding is that activation energy of chemical reaction remarkably alters the solute concentration near the plate.

Keywords Generalized Newtonian fluid · Chemical reaction · Activation energy · Falkner–Skan flow

List of Symbols

(x, y)	Cartesian coordinate system
u, v	Velocity components along x- and y-directions, respectively
K	Consistency index
f	Dimensionless stream function
B_0	Magnetic flux density
a	Positive constant
M	Magnetic interaction parameter
c_p	Specific heat
$k(T)$	Variable thermal conductivity
n	Flow behavior index
E_a	Activation energy
m	Fitted rate constant
s	Heat source/sink
E	Dimensionless activation energy
Pr	Prandtl number
Re_x	Local Reynolds number
We	Local Weissenberg number
Sc	Schmidt number
T	Fluid temperature
C	Solute concentration
C_f	Skin friction coefficient
Nu_x	Local Nusselt number
Sh_x	Local Sherwood number
τ_w	Shear stress at the plate
q_w	Wall heat flux
j_w	Wall mass flux
$u_e(x)$	Velocity of the outer flow

Greek Symbols

$\dot{\gamma}$	Shear rate
η	Similarity variable
θ	Dimensionless temperature
ϕ	Dimensionless concentration
η_0	Viscosity at zero shear rate
η_∞	Infinite shear rate viscosity
δ	Temperature difference parameter
σ_1	Fluid electrical conductivity
ϵ	Dimensionless constant
ρ	Fluid density
κ	Boltzmann constant
σ	Dimensionless reaction parameter

✉ M. Mustafa
meraj_mm@hotmail.com

[1] School of Natural Sciences (SNS), National University of Sciences and Technology (NUST), Islamabad 44000, Pakistan

[2] Higher Colleges of Technology (HCT), Abu Dhabi 5464, United Arab Emirates

1 Introduction

There exists a large class of substances for which mechanical properties deviate from the usual Newtonian constitutive relation to a greater or lesser extent. In generalized Newtonian fluids, the components of stress tensor and those of strain rate tensor are proportional, but proportionality factor is a function of scalar invariants of strain rate tensor itself. However, such fluids are incapable of detecting normal stress phenomena such as rod climbing effect or dye swelling and time-dependent effects associated with the viscoelastic properties of a fluid. Power-law fluid model [1] is widely regarded as the most convenient form for describing shear-thinning/shear-thickening flow phenomena in many fluids including polymeric solutions and melts, dispersions and weak gels. However, this model is inadequate when the experimental data are obtained over a wide range of shear rates. In such cases, one must resort to four-parameter Cross [2] and Carreau [3] rheological models. These models have been found appropriate in predicting shear-thinning effects for both low and high shear rates. Xie and Jin [4] explored Cross fluid model for a non-Newtonian flow problem using a numerical scheme. Khan et al. [5] modeled effect of activation energy on flow of shear-thinning fluid in the region of stagnation point utilizing Cross rheological equation. Khan et al. [6] used Cross model to analyze momentum and heat transport above a radially expanding disk. Very recently, temperature-dependent chemical reaction in Cross fluid flow with nanoparticles has been investigated numerically by Khan et al. [7].

Modeling transfer of heat and chemically reactive substances in fluid flow has essence in wide-ranging processes in chemical industries including condensation, vaporization, diffusion, alcohol distillation, gas absorption and applications in oil reservoirs, nuclear reactor cooling and much more. In particular, temperature-dependent reaction rate becomes important in processes involving geothermal and oil reservoir engineering and in understanding the dynamics of water and oil emulsions. In recent years, vast wealth of material concerning fluid flow comprising chemically reactive substances has been published. For example, Siddiqa et al. [8] found locally similar solutions for buoyancy assisted flow in the existence of heat/mass transfer effects. Maxwell fluid flow along a stretchable surface comprising reactive nanoparticles was examined by Afify and Elgazery [9] using a numerical approach. Zhuang et al. [10] considered double diffusion in a power-law fluid flow through a porous space with chemical reaction. A numerical study describing the flow of non-Newtonian Sisko fluid near a cylindrical surface influenced by chemical reaction was conducted by Malik and Khan [11]. The effect of chemically reacting solute on unsteady non-Newtonian fluid between a squeezing channel was investigated by Adesanya et al. [12]. Hayat et al. [13] also examined chemical reaction effects on MHD flow between rotating porous disks using analytical approach. Similar attempts in this direction can be pursued through [14–19] and references there in.

Activation energy is the minimum amount of energy required by the reactants to experience a chemical reaction. The source of activation energy required to initiate chemical reactions is typical heat energy from the surroundings. Bestman [20] analyzed natural convective flow of binary mixture over a moving permeable wall using a perturbation scheme. Maleque et al. [21] utilized modified Arrhenius function to model the onset of activation energy on MHD flow induced by a moving plate. In another study, Maleque et al. [22] explored natural convection along a permeable surface when chemical reaction rate depends on the activation energy. Awad et al. [23] explored activation energy aspect for unsteady flow of binary fluid in rotating frame. Later, Shafique et al. [24] also made use of Arrhenius function to model mass transport in binary viscoelastic fluid flow subject to rotating frame. Recently published reports in this domain can be found in Refs. [25–28].

Here our intention is to model the non-Newtonian fluid flow near a rigid plate caused by stream-wise pressure gradient when Cross rheological equation is involved. In this work, variation in fluid thermal conductivity with absolute temperature is considered. Furthermore, the flow field is assumed to contain chemically reacting species. Furthermore, mass transfer process is formulated via modified Arrhenius function for activation energy. Subsequent section covers problem formulation using boundary layer approximations. Numerical method of solution is explained next. Results addressing the behaviors of pertinent parameters are discussed in the next section. Finally, the work is concluded by highlighting major outcomes of the study.

2 Problem Formulation

Let us consider a flow of shear-thinning fluid obeying Cross rheological model along a flat plate with variable external free stream. The plate resides along the x-axis and fluid occupies the region $y \geq 0$. Let T_w be the constant temperature at the plate and C_w be the solute concentration at the plate. The ambient temperature and solute concentration, denoted by T_∞ and C_∞, respectively, are attained high above the plate. Activation energy due to modified Arrhenius function will be considered here. Flow field exhibits the influence of transverse magnetic field. Invoking customary assumption of low magnetic Reynolds number, the induced magnetic field becomes negligible in comparison with applied magnetic field. The electric field is assumed absent. Cross [2] proposed the following rheological equation of state for shear-thinning fluids:

$$\frac{\eta-\eta_\infty}{\eta_0-\eta_\infty}=\left(\frac{1}{1+(K\,|\dot{\gamma}|)^n}\right), \tag{1}$$

where η_0 is the viscosity at zero shear rate, η_∞ is the infinite shear rate viscosity which will be neglected here, K stands for the consistency index, $\dot{\gamma}$ denotes the shear rate and n is the flow behavior index of the fluid.

Accounting (1), the extra stress tensor can be expressed as:

$$\mathbf{S}=\eta\mathbf{A_1}=\left(\frac{\eta_0}{1+(K\,|\dot{\gamma}|)^n}\right)\mathbf{A_1}, \tag{2}$$

where $\mathbf{A_1}=(\nabla\mathbf{V})+(\nabla\mathbf{V})^{\mathbf{t}}$ the first Rivlin–Ericksen tensor. In view of the aforementioned assumptions, flow, heat and mass transfer are governed by the following equations:

$$\frac{\partial u}{\partial x}+\frac{\partial v}{\partial y}=0, \tag{3}$$

$$u\frac{\partial u}{\partial x}+v\frac{\partial u}{\partial y}=u_e\frac{\mathrm{d}u_e}{\mathrm{d}x}+\nu\frac{\partial}{\partial y}\left(\frac{\frac{\partial u}{\partial y}}{1+\left(K\left|\frac{\partial u}{\partial y}\right|\right)^n}\right)+\frac{\sigma_1 B_0^2}{\rho}\left(u_e-u\right), \tag{4}$$

$$\rho c_p\left(u\frac{\partial T}{\partial x}+v\frac{\partial T}{\partial y}\right)=\frac{\partial}{\partial y}\left(k\left(T\right)\frac{\partial T}{\partial y}\right)+Q\left(T-T_\infty\right), \tag{5}$$

$$u\frac{\partial C}{\partial x}+v\frac{\partial C}{\partial y}=D\nabla^2 C-k_r^2\left(\frac{T}{T_\infty}\right)^m e^{\frac{-E_a}{\kappa T}}\left(C-C_\infty\right). \tag{6}$$

With no slip and no penetration at the plate, one can write:

$$u=0,\ v=0,\ T=T_w,\ C=C_w \text{ at } y=0, \tag{7a}$$

and at the frictionless regime, we have:

$$u\to u_e\left(x\right)=ax, v\to v_e\left(y\right)=-ay,$$
$$T\to T_\infty, C\to C_\infty \text{as} y\to\infty, \tag{7b}$$

where $\nu=\eta_0/\rho$ denotes the kinematic viscosity in which ρ is the fluid density, $\sigma^\star$ represents the fluid electrical conductivity, B_0 denotes the constant magnetic flux density, c_p the specific heat capacity, $k\left(T\right)=k_\infty\left(1+\epsilon\left(T-T_\infty\right)/\Delta T\right)$ the thermal conductivity in which k_∞ denotes thermal conductivity at the ambient and $\epsilon>0$ is a constant [28].

The term $Q\left(T-T_\infty\right)$ measures the amount of heat transferred per unit volume where Q is a constant. The term $k_r^2(T/T_\infty)^m e^{-E_a/\kappa T}$ represents temperature-dependent reaction rate in which E_a denotes the activation energy, $\kappa=8.61\times10^{-5}$eV/K the Boltzmann constant and $m\in(-1,1)$ the fitted rate constant.

Let us introduce the transformations

$$\eta=\left(\frac{u_e}{x\nu}\right)^{\frac{1}{2}}y, u=u_e f'\left(\eta\right), v=-\left(\frac{\nu u_e}{x}\right)^{\frac{1}{2}}f\left(\eta\right),$$

$$\theta\left(\eta\right)=\frac{T-T_\infty}{T_w-T_\infty},\quad \phi\left(\eta\right)=\frac{C-C_\infty}{C_w-C_\infty}, \tag{8}$$

where $f\left(\eta\right)$ is the non-dimensional stream function, $\theta\left(\eta\right)$ the non-dimensional temperature and $\phi(\eta)$ represents the non-dimensional concentration; the continuity equation (3) is fulfilled, while Eqs. (4)–(6) convert into the following ODEs:

$$f'''+\frac{\left[1+\left(We\left|f''\right|\right)^n\right]^2}{\left[1+(1-n)\left(We\left|f''\right|\right)^n\right]}\left[ff''-f'2+M^2\left(1-f'\right)+1\right]=0, \tag{9}$$

$$(1+\epsilon\theta)\,\theta''+\epsilon\theta'^2+Pr\left(f\theta'+s\theta\right)=0, \tag{10}$$

$$\phi''+Scf\phi'-Sc\sigma\left(1+\delta\theta\right)^m e^{-\left(\frac{E}{1+\delta\theta}\right)}\phi=0. \tag{11}$$

The boundary conditions (7a) and (7b) are transformed as

$$f\left(0\right)=0,\ f'\left(0\right)=0,\theta\left(0\right)=1,\phi\left(0\right)=1, \tag{12a}$$

$$f'\to1,\theta\to0,\phi\to0\text{as}\eta\to\infty. \tag{12b}$$

In Eqs. (9)–(11), $We=aK\left(Re_x\right)^{1/2}$ denotes the local Weissenberg number in which $Re_x=u_e x/\nu$ denotes the local Reynolds number, $M=\left(\sigma_1 B_0^2/\rho a\right)^{1/2}$ represents the magnetic interaction parameter, $s=Q/a\rho c_p$ for the heat source/sink parameter, $Sc=\nu/D$ for Schmidt number, $\sigma=k_r^2/a$ is the dimensionless reaction parameter, $\delta=\Delta T/T_\infty$ is the temperature difference parameter, $E=E_a/(\kappa T_\infty)$ denotes the dimensionless activation energy and $Pr=\eta_0 c_p/k_\infty$ stands for Prandtl number. Note that the Prandtl number is clearly a constant since k_∞ is the thermal conductivity at the ambient, which is constant. Hence, consideration of similarity transformation allows us to get away with the difficulty of varying Prandtl number. A detailed clarification on the subject (in case of variable viscosity) has already been provided by Andersson et al. [29].

We are primarily interested in evaluating local Skin friction coefficientC_f at the plate defined by:

$$C_f=\frac{\tau_w}{\rho u_e^2/2}, \tag{13}$$

where τ_w denotes shear stress at the plate which is obtained as follows:

$$\tau_w=\tau_{xy}\big|_{y=0}=\eta_0\left(\frac{\frac{\partial u}{\partial y}}{1+\left(K\left|\frac{\partial u}{\partial y}\right|\right)^n}\right)_{y=0}$$
$$=\eta_0\left(\frac{a\left(Re_x\right)^{\frac{1}{2}}}{1+\left(We f''(0)\right)^n}\right). \tag{14}$$

Using Eq. (14) and the transformations (8), Eq. (14) takes the following form:

$$\frac{1}{2} Re_x^{\frac{1}{2}} C_f = \frac{f''(0)}{1 + (We\,|f''(0)|)^n}, \tag{15}$$

in which $Re_x = u_e x/\nu$ is the local Reynolds number.

In order to compute heat and mass transfer rates from the solid surface, we define local Nusselt number Nu_x and local Sherwood number Sh_x:

$$Nu_x = \frac{x q_w}{k(T_w - T_\infty)}, \; Sh_x = \frac{x j_w}{D(C_w - C_\infty)} \tag{16}$$

where $q_w = -k\,(\partial T/\partial y)_{y=0}$ is the wall heat flux and $j_w = -D\,(\partial C/\partial y)_{y=0}$ denotes wall mass flux. Inserting these expressions in Eq. (16) and then using transformations (8), it is easy to verify that:

$$Re_x^{-\frac{1}{2}} Nu_x = -\theta'(0)\,, \; Re_x^{-\frac{1}{2}} Sh_x = -\phi'(0)\,. \tag{17}$$

3 Method of Solution

The differential system posed by Eqs. (9)–(11) subject to the conditions (12a) and (12b) has been solved numerically by employing MATLAB package bvp4c that is known for producing accurate numerical results for multipoint boundary value problems. To begin, we reduce the system (9)–(11) into a first-order system by substituting $y_1 = f$, $y_2 = f'$, $y_3 = f''$, $y_4 = \theta$, $y_5 = \theta'$, $y_6 = \phi$ and $y_7 = \phi'$. We obtain the following:

$$y_1' = y_2, \tag{18}$$

$$y_2' = y_3, \tag{19}$$

$$y_3' = -\frac{\left\{1 + (We\,|y_3|)^n\right\}^2}{\left\{1 + (1-n)\,(We\,|y_3|)^n\right\}} \left\{y_1 y_3 - y_2^2 + M^2\,(1 - y_2) + 1\right\}, \tag{20}$$

$$y_4' = y_5, \tag{21}$$

$$y_5' = -\frac{1}{(1 + \epsilon y_4)} \left\{\epsilon y_4^2 + Pr\,(y_1 y_5 - s y_4)\right\}, \tag{22}$$

$$y_6' = y_7, \tag{23}$$

$$y_7' = -Sc \left\{y_1 y_7 - \sigma\,(1+\delta y_4)^m \exp\left(\frac{-E}{1+\delta y_4}\right) y_6\right\}. \tag{24}$$

The above set of equations with the respective conditions are directly substituted in solver bvp4c. The residual of the boundary conditions is chosen to be uniformly small. For detailed implementation of the solver bvp4c, the reader is referred to Ref. [30].

4 Results and Discussion

In this section, our interest is to envisage the role of embedded physical parameters on the solutions by presenting graphical illustrations. Figure 1 demonstrates the variation in u velocity component with vertical distance η for various values of Weissenberg number We. Intriguingly, the profile of f' has similar trends in both Newtonian ($We = 0$) and non-Newtonian ($We \neq 0$) fluids. The function f' is zero at the plate and tends to unity as $\eta \to \infty$. It is clear that by increasing Weissenberg number, the boundary layer thickness reduces sharply. This reduction is accompanied by a higher value of wall velocity gradient $f''(0)$. Figure 2 indicates that boundary layer effects extend up to higher vertical distance when larger flow behavior index n is considered. Such outcome suggests that skin friction coefficient can be lowered by increasing value of n. Such behavior is reminiscent of shear-thinning characteristic of Cross fluid. In Fig. 3, we plot u velocity component f' versus η for varying values of magnetic interaction parameter M. In the existence of magnetic field, the boundary layer thickness is significantly diminished compared with the same without any magnetic field. Thus, we anticipate wall shear to enhance as parameter M becomes large. Consequently, the function f' increases upon increasing magnetic field strength. Physically Lorentz force established as a result of transverse magnetic field resists the momentum transport due to which boundary layer suppresses.

Our computations detect that v—velocity component, represented by f—also enhances with increasing parameter M. This in turn increases the amount of cold fluid drawn toward the plate due to which thermal boundary layer suppresses (see Fig. 4). In Fig. 5, temperature curves are computed for a wide range of heat source/sink parameters s. An expansion in thermal boundary layer becomes apparent as parameter ($s > 0$) becomes large. However, opposite trend is detected by

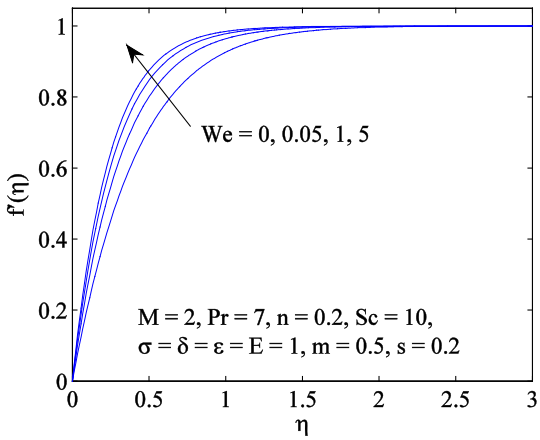

Fig. 1 Variation in $f'(\eta)$ with η for various values of local Weissenberg number We

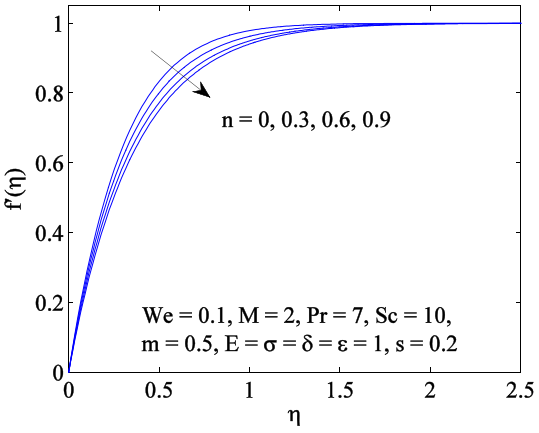

Fig. 2 Variation in $f'(\eta)$ with η for different values of flow behavior index n

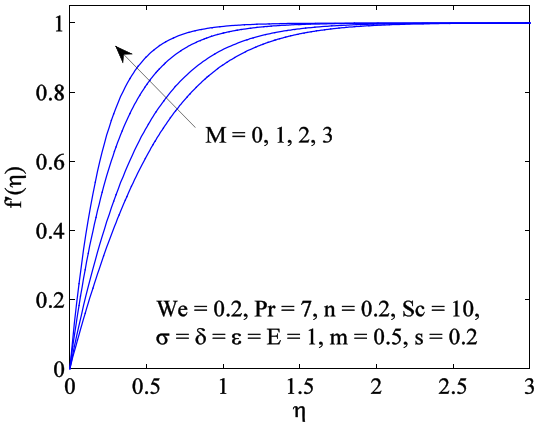

Fig. 3 Variation in $f'(\eta)$ with η for various values of magnetic interaction parameter M

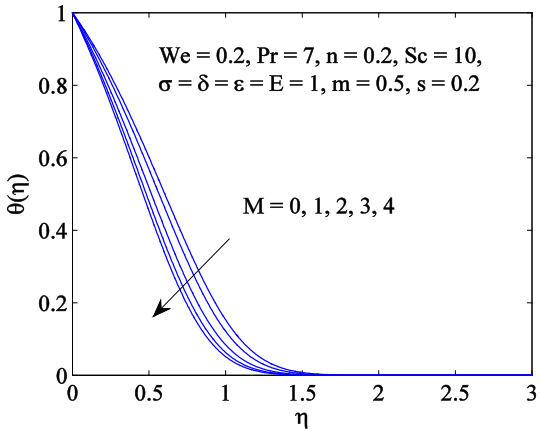

Fig. 4 Variation in $\theta(\eta)$ with η for various values of magnetic interaction parameter M

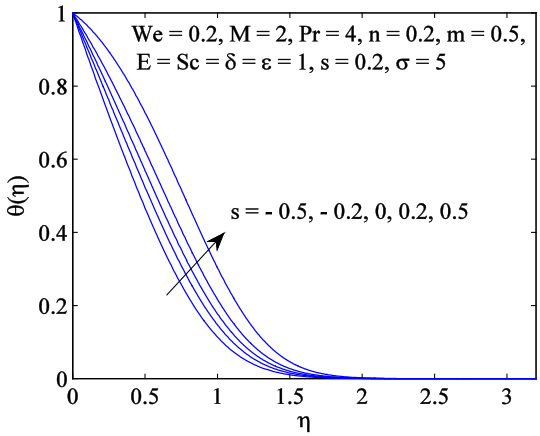

Fig. 5 Variation in $\theta(\eta)$ with η for various values of heat source/sink parameter s

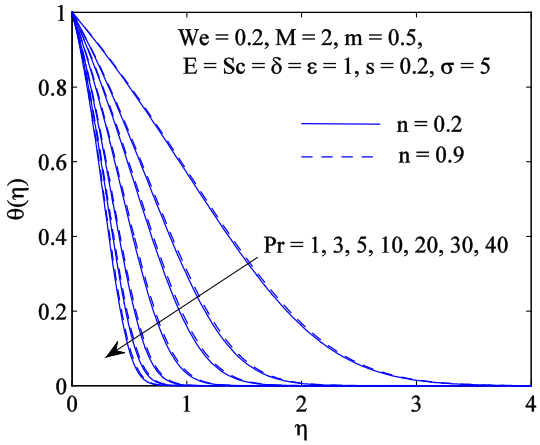

Fig. 6 Variation in $\theta(\eta)$ with η for various values of Prandtl number Pr

increasing heat sink parameter ($s < 0$). Therefore, we conclude that heat transfer from the plate improves/deteriorates as heat sink/source effect intensifies. Figure 6 portrays the change in temperature profile with η at a variety of Prandtl numbers. By increasing Prandtl number, momentum diffusion effect becomes strong in comparison with the thermal diffusion which leads to the thinning of thermal penetration depth and improvement in heat transfer rate from solid boundary. Figure 7 displays the variation in temperature profile $\theta(\eta)$ by changing the parameter ϵ. Thermal conductivity expression suggests that thermal conductivity varies linearly within the boundary layer with change in temperature. Thus, higher value of ϵ leads to a pronounced heat conduction and reduced magnitude of local Nusselt number.

Figure 8 demonstrates the effect of reaction rate parameter σ on concentration profile $\phi(\eta)$. The general trend of concentration ϕ is analogous to that of temperature θ in nearly all the cases. As anticipated, solute concentration is diminished within the boundary layer as generative reaction rate is increased. Figure 9 shows the evolution of concentration profile at a variety of Schmidt numbers. Concentration boundary layer shrinks as Schmidt number Sc becomes large. Physically, an increase in Sc implies a reduction in mass dif-

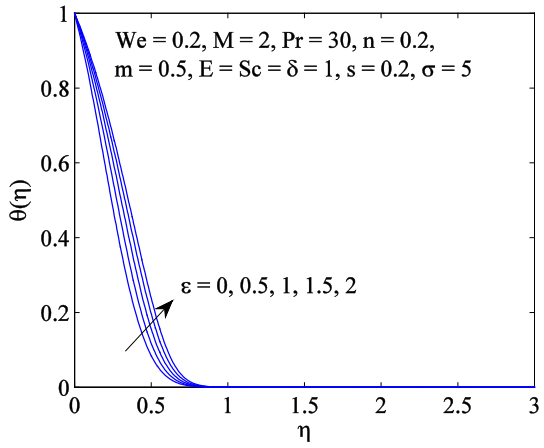

Fig. 7 Variation in $\theta(\eta)$ with η for various values of parameter ϵ

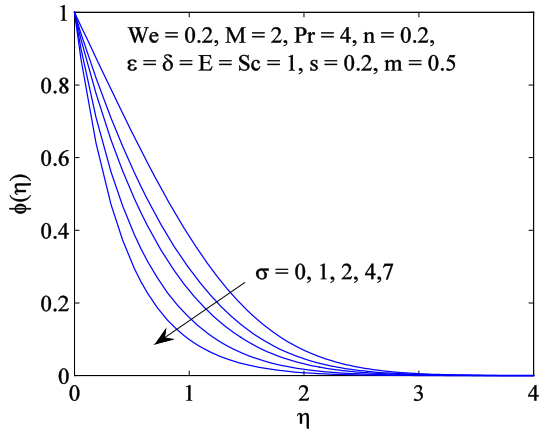

Fig. 8 Variation in $\phi(\eta)$ with η for various values of parameter σ

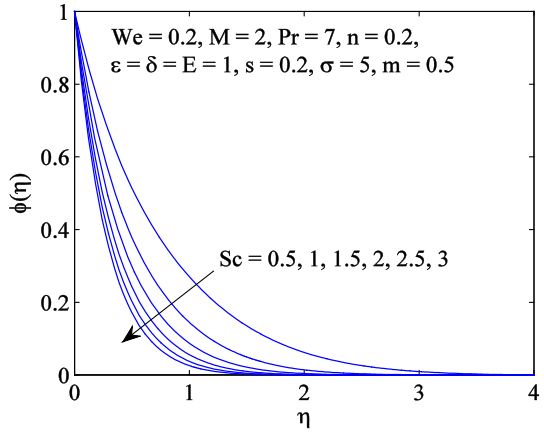

Fig. 9 Variation in $\phi(\eta)$ with η for various values of Schmidt number Sc

fusivity which results in enhanced mass transfer of solute from the plate resulting into higher concentration gradient at the plate surface. To envisage the role of fitted rate constant m in the development of concentration boundary layer, Fig. 10 is prepared. It appears that behavior of m on ϕ is

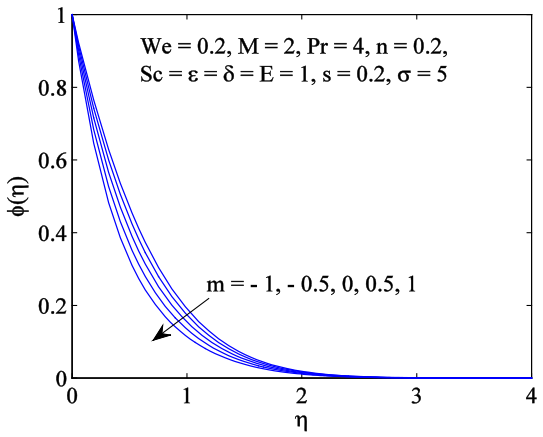

Fig. 10 Variation in $\phi(\eta)$ with η for various values of fitted rate constant m

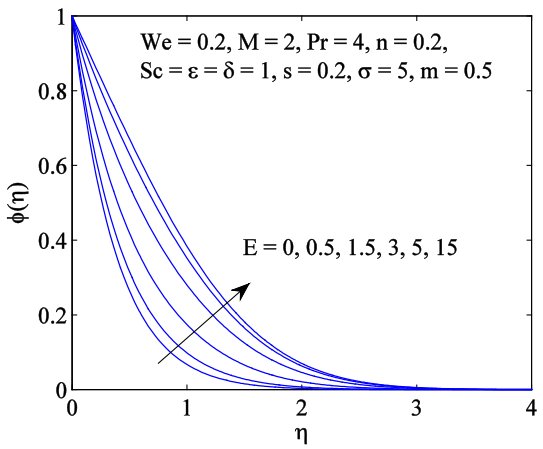

Fig. 11 Variation in $\phi(\eta)$ with η for various values of activation energy E

qualitatively similar to that of σ. Activation energy refers to the least amount of energy required to initiate chemical reaction. Modified Arrhenius function $k_r^2\,(T/T_\infty)^m\, e^{\frac{-E_a}{kT}}$, representing reaction rate, is expected to decrease/increase with increasing activation energy/fluid temperature. It can be noted that the reaction rate given by Arrhenius function is exponentially decaying function of E_a or E. When E/δ becomes large, that is, $E/\delta \to \infty$, the reaction rate represented by Arrhenius function vanishes. As a result, the concentration profile ϕ reaches a constant solution as E/δ gets large. Further, as $E/\delta \to 0$ or equivalently $E \to 0$, the reaction rate varies substantially with temperature when compared with E_a. A solution for $E = 0$ is also included in Fig. 11. In Fig. 12, the variation in ϕ with increasing parameter δ is portrayed. By increasing this parameter, wall and ambient temperature difference enlarges which leads to a pronounced heat transfer. Importance of Arrhenius function, therefore, increases with increasing δ which in turn leads to a reduction in concentration boundary layer thickness.

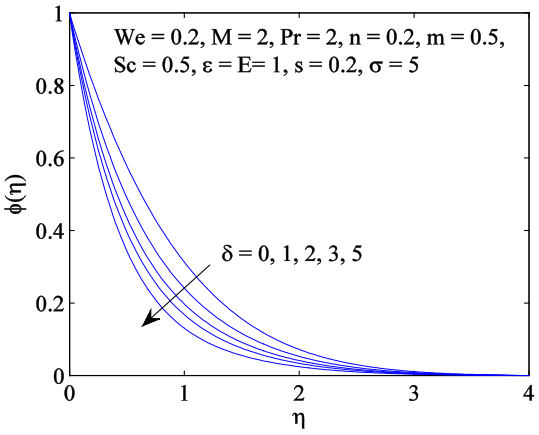

Fig. 12 Variation in $\phi\ (\eta)$ with η for various values of δ

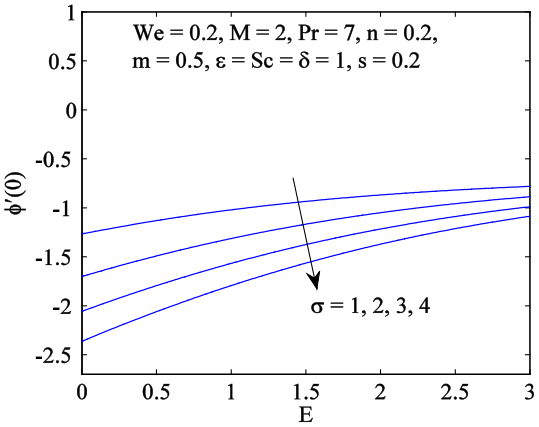

Fig. 13 Variation in $\phi'(0)$ with E for various values of σ

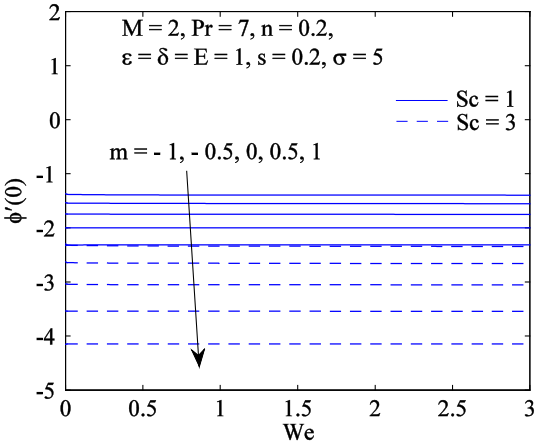

Fig. 14 Variation in $\phi'(0)$ with We for various values of m

Figures 13 and 14 show the influences of Weissenberg number We and activation energy on local Sherwood number. The absolute value of $\phi'(0)$ approaches a constant value as activation energy for chemical reaction becomes large. The parameter σ is seen to enhance the mass transfer rate from the plate. Note that the fitted rate constant m also boosts the mass transfer rate.

Table 1 Computational results of local Nusselt number for varying values of We and n with $\sigma = \delta = E = Sc = \epsilon = 1$, $m = 0.5$, $s = 0.2$ and $Pr = 5$

We	n	$Re_x^{-\frac{1}{2}} Nu_x$
0.1	0.2	0.65752
0.3		0.66842
0.5		0.67388
0.7		0.67761
0.2	0.1	0.66674
	0.3	0.66174
	0.5	0.65647
	0.7	0.65093

Table 2 Computational results of local Sherwood number for varying values of σ, δ, E, Sc, m when $We = 0.2$, $n = 0.2$, $M = 2$, $s = 0.2$ and $\epsilon = 1$

σ	δ	E	Sc	m	$Re_x^{-\frac{1}{2}} Sh_x$
0	1	1	1	0.5	0.66637
1					1.02822
2					1.32638
3					1.58330
1	0				0.86964
	2				1.15121
	3				1.25080
	4				1.33470
	1	0			1.27215
		2			0.87439
		3			0.78405
		4			0.73273
		5			0.70389
		1	2		1.44872
			3		1.76654
			4		2.03170
			5		2.26353
			1	-1	0.85029
				-0.5	0.89489
				0	0.95286
				1	1.12611
				0.5	1.02425

Table 1 includes the local Nusselt number data obtained by varying the rheological parameters of Cross fluid model. Heat transfer rate is slightly reduced as the flow behavior index n enlarges. A modest elevation in heat transfer rate is also depicted for increasing fluid relaxation time.

In Table 2, we enlist the data of local Sherwood number found by varying embedded parameters. Increasing trend in local Sherwood number is observed when either chemical reaction rate or wall and ambient temperature difference

enlarges. Similar behavior is noticed when Schmidt number becomes large. As Schmidt number Sc gradually increases, the relative importance of momentum diffusion reduces and, as a consequence, mass transfer rate is lowered. However, mass transfer rate is substantially elevated as activation energy for chemical reaction enlarges. Further, our computations illustrate that the impacts of Activation energy E and chemical reaction rate σ on solution profiles and local Sherwood number remain similar even in the Newtonian fluid case, for which solutions are self-similar. This outcome depicts that physical outcomes concerning the behaviors of embedded parameters appear to be same in both self-similar and locally similar cases. This can also be seen by comparing the velocity profiles for $We = 0$ and $We \neq 0$.

5 Concluding Remarks

Boundary layer flow of Cross rheological fluid along a static plate with stream-wise pressure gradient is addressed in this paper. The flow field is influenced by chemically reactive species. Modified Arrhenius function is introduced in order to account for temperature dependency of reaction rate on activation energy. Accurate numerical calculations are made for a full range of embedded parameters. Main outcomes of this analysis are listed as follows:

- At a point inside the boundary layer, heat source parameter ($s > 0$) enhances fluid temperature, whereas heat sink parameter ($s < 0$) does the reverse.
- By increasing shear-thinning parameter n, drag forces reduce, thereby favoring the momentum transport above the surface. Consequently, boundary layer effects extend up to a higher axial distance when larger value of n is considered.
- The expression of thermal conductivity $k(T)$ predicts that by increasing parameter ϵ, heat penetration depth would enhance. As a result, temperature profile becomes thicker as parameter ϵ becomes large.
- By increasing the parameter E, the (destructive) reaction rate slows down, and hence, an enhancement in concentration boundary layer occurs.
- The vertical velocity v at infinity grows with increasing shear-thinning parameter n. This eventually increases the amount of cold fluid drawn toward the stretching sheet. As a consequence, thermal boundary layer expands as shear-thinning effect is strengthened.
- By increasing reaction parameter σ, reaction rate amplifies which in turn reduces the concentration of chemical species present inside the boundary layer. That is why, concentration layer suppresses as reaction parameter σ becomes large.

References

1. Bird, R.B.; Curtiss, C.F.; Armstrong, R.C.; Hassager, O.: Dynamics of Polymeric Liquids. Wiley, Newyork (1987)
2. Cross, M.M.: Rheology of non-Newtonian fluids: a new flow equation for pseudoplastic systems. J. Colloid Sci. **20**, 417–437 (1965)
3. Carreau, P.J.: Rheological equations from molecular network theories. Trans. Soc. Rheol. **116**, 99–127 (1972)
4. Xie, J.; Jin, Y.C.: Parameter determination for the Cross rheology equation and its application to modeling non-Newtonian flows using the WC-MPS method. Eng. Appl. Comput. Fluid Mech. **10**, 111–129 (2016)
5. Khan, M.I.; Waqas, M.; Hayat, T.; Alsaedi, A.: Magneto-hydrodynamical numerical simulation of heat transfer in MHD stagnation point flow of Cross fluid model towards a stretched surface. Phys. Chem. Liq. **7**, 1824–1827 (2017). https://doi.org/10.1080/00319104.2017.1367791
6. Khan, M.; Manzoor, M.; Rahman, M.: On axisymmetric flow and heat transfer of Cross fluid over a radially stretching sheet. Res. Phys. **7**, 3767–3772 (2017)
7. Khan, M.I.; Hayat, T.; Khan, M.I.; Alsaedi, A.: Activation energy impact in nonlinear radiative stagnation point flow of Cross nanofluid. Int. Commun. Heat Mass Transf. **91**, 216–224 (2018)
8. Siddiqa, S.; Hossain, M.A.; Pop, I.: Conjugate thermal and mass diffusion effect on natural convection flow in presence of strong cross magnetic field. Int. J. Heat Mass Transf. **55**, 5120–5132 (2012)
9. Afify, A.; Elgazery, N.S.: Effect of a chemical reaction on magnetohydrodynamic boundary layer flow of a Maxwell fluid over a stretching sheet with nanoparticles. Particuology **29**, 154–161 (2016)
10. Zhuang, Y.H.; Yu, H.Z.; Zhu, Q.Y.: A thermal non-equilibrium model for 3D double diffusive convection of power-law fluids with chemical reaction in the porous medium. Int. J. Heat Mass Transf. **115**, 670–694 (2017)
11. Malik, R.; Khan, M.: Numerical study of homogeneous-heterogeneous reactions in Sisko fluid flow past a stretching cylinder. Res. Phys. **8**, 64–70 (2018)
12. Hayat, T.; Khan, M.W.A.; Khan, M.I.; Waqas, M.; Alsaedi, A.: Impact of chemical reaction in fully developed radiated mixed convective flow between two rotating disk. Physica B: Cond. Matter **538**, 138–149 (2018)
13. Adesanya, S.O.; Ogunseye, H.A.; Jangili, S.: Unsteady squeezing flow of a radiative Eyring–Powell fluid channel flow with chemical reactions. Int. J. Thermal Sci. **125**, 440–447 (2018)
14. Hayat, T.; Waqas, M.; Ijaz Khan, M.; Alsaedi, A.: Impacts of constructive and destructive chemical reactions in magnetohydrodynamic (MHD) flow of Jeffrey liquid due to nonlinear radially stretched surface. J. Mol. Liq. **225**, 302–310 (2017)
15. Lu, J.; Das, S.; Peters, E.A.J.F.; Kuipers, J.A.M.: Direct numerical simulation of fluid flow and mass transfer in dense fluid-particle systems with surface reactions. Chem. Eng. Sci. **176**, 1–18 (2018)
16. Hashim, M.Khan; Alshomrani, A.S.; Haq, R.: Investigation of dual solutions in flow of a non-Newtonian fluid with homogeneous–heterogeneous reactions: critical points. Eur. J. Mech. B/Fluids **68**, 30–38 (2018)
17. Turkyilmazoglu, M.: Analytical solutions to mixed convection MHD fluid flow induced by a nonlinearly deforming permeable surface, Commun. Nonlinear Sci. Numer. Simul. In press (2018). https://doi.org/10.1016/j.cnsns.2018.04.002
18. Khan, J.A.; Mustafa, M.: A numerical analysis for non-linear radiation in MHD flow around a cylindrical surface with chemically reactive species. Res. Phys. **8**, 963–970 (2018)
19. Lu, D.C.; Ramzan, M.; Bilal, M.; Chung, J.D.; Farooq, U.: A numerical investigation of 3D MHD rotating flow with binary

chemical reaction, activation energy and non-fourier heat flux. Commun. Theor. Phys. **70**, 89–96 (2018)
20. Bestman, R.: Natural convection boundary layer with suction and mass transfer in a porous medium. Int. J. Energy Res. **14**, 389–396 (1990)
21. Maleque, K. A.: Effects of binary chemical reaction and activation energy on MHD boundary layer heat and mass transfer flow with viscous dissipation and heat generation/absorption, ISRN Thermodyn. 2013 (2013), Article ID 284637. https://doi.org/10.1155/2013/284637
22. Maleque, K.A.: Effects of exothermic/endothermic chemical reactions with Arrhenius activation energy on MHD free convection and mass transfer flow in presence of thermal radiation. J. Thermodyn. 2013 (2013), Article ID 629516. https://doi.org/10.1155/2013/692516
23. Awad, F.G.; Motsa, S.; Khumalo, M.: Heat and mass transfer in unsteady rotating fluid flow with binary chemical reaction and activation energy. PloS One **9**, e107622 (2014). https://doi.org/10.1371/journal.pone.0107622
24. Shafique, Z.; Mustafa, M.; Mushtaq, A.: Boundary layer flow of Maxwell fluid in rotating frame with binary chemical reaction and activation energy. Res. Phys. **6**, 627–633 (2016)
25. Abbas, Z.; Sheikh, M.; Motsa, S.S.: Numerical solution of binary chemical reaction on stagnation-point flow of Casson fluid over a stretching/shrinking sheet with thermal radiation. Energy **95**, 12–20 (2016)
26. Mustafa, M.; Mushtaq, A.; Hayat, T.; Alsaedi, A.: Numerical study of MHD viscoelastic fluid flow with binary chemical reaction and Arrhenius activation energy. Int. J. Chem. React. Eng. 15 (2016). https://doi.org/10.1515/ijcre-2016-0131.
27. Mustafa, M.; Khan, J.A.; Hayat, T.; Alsaedi, A.: Buoyancy effects on MHD nanofluid flow past a vertical surface with chemical reaction and activation energy. Int. J. Heat Mass Transf. **108**, 1340–1346 (2017)
28. Ramzan, M.; Bilal, M.; Kanwal, S.; Chung, J.D.: Effects of variable thermal conductivity and non-linear thermal radiation past an Eyring–Powell nanofluid flow with chemical reaction. Commun. Theor. Phys. **67**, 723–731 (2017)
29. Andersson, H.I.; Aarseth, J.B.: Sakiadis flow with variable fluid properties revisited. Int. J. Eng. Sci. **45**, 554–661 (2007)
30. Shampine, L. F.; Reichelt, M. W.; Kierzenka, J.: Solving boundary value problems for ordinary differential equations in MATLAB with bvp4c. https://www.mathworks.com/help/matlab/ref/bvp4c.html